

Photochemical Route to Actinide-Transition Metal Bonds: Synthesis, Characterization and Reactivity of a Series of Thorium and Uranium Heterobimetallic Complexes

Ashleigh L. Ward,^{†,‡} Wayne W. Lukens,[‡] Connie C. Lu,[§] and John Arnold^{*,†,‡}

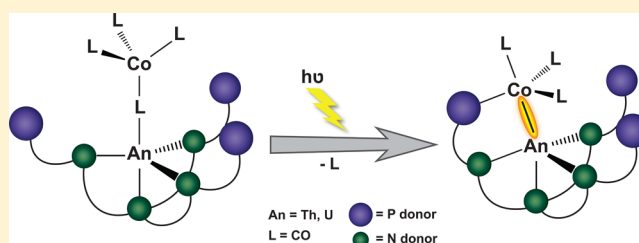
[†]Department of Chemistry, University of California, Berkeley, California 94720, United States

[‡]Chemical Sciences Division, Lawrence Berkeley National Lab, Berkeley, California 94720, United States

[§]Department of Chemistry, University of Minnesota, Minneapolis, Minnesota 55455, United States

Supporting Information

ABSTRACT: A series of actinide–transition metal heterobimetallics has been prepared, featuring thorium, uranium, and cobalt. Complexes incorporating the binucleating ligand N[*o*-(NHCH₂PⁱPr₂)C₆H₄]₃ with either Th(IV) (4) or U(IV) (5) and a carbonyl bridged [Co(CO)₄][−] unit were synthesized from the corresponding actinide chlorides (Th: 2; U: 3) and Na[Co(CO)₄]. Irradiation of the resulting isocarbonyls with ultraviolet light resulted in the formation of new species containing actinide–metal bonds in good yields (Th: 6; U: 7); this photolysis method provides a new approach to a relatively unusual class of complexes. Characterization by single-crystal X-ray diffraction revealed that elimination of the bridging carbonyl and formation of the metal–metal bond is accompanied by coordination of a phosphine arm from the N₄P₃ ligand to the cobalt center. Additionally, actinide–cobalt bonds of 3.0771(5) Å and 3.0319(7) Å for the thorium and uranium complexes, respectively, were observed. The solution-state behavior of the thorium complexes was evaluated using ¹H, ¹H–¹H COSY, ³¹P, and variable-temperature NMR spectroscopy. IR, UV–vis/NIR, and variable-temperature magnetic susceptibility measurements are also reported.



INTRODUCTION

Probing the nature of bonds formed between actinide metals and other elements is important for expanding our understanding of the electronic structure and chemical bonding of the *f*-block elements, and in turn driving its evolution.^{1–7} In the case of metal–metal bonds, those involving the *5f* elements are fundamentally different from their transition metal and lanthanide counterparts as a result of actinide *f* orbital participation in bonding, coordinative diversity, and access to a wide range of oxidation states.^{1,8} Understanding these fundamental properties is of importance in nuclear fuel technologies, where small differences in covalency between the *4f* and *5f* elements may provide opportunities to improve fission product separations.^{9–12} Additionally, novel applications utilizing the actinides have recently emerged, including hydrocarbon functionalization, small-molecule activation, and group atom transfer reactions facilitated by uranium catalysts.¹³

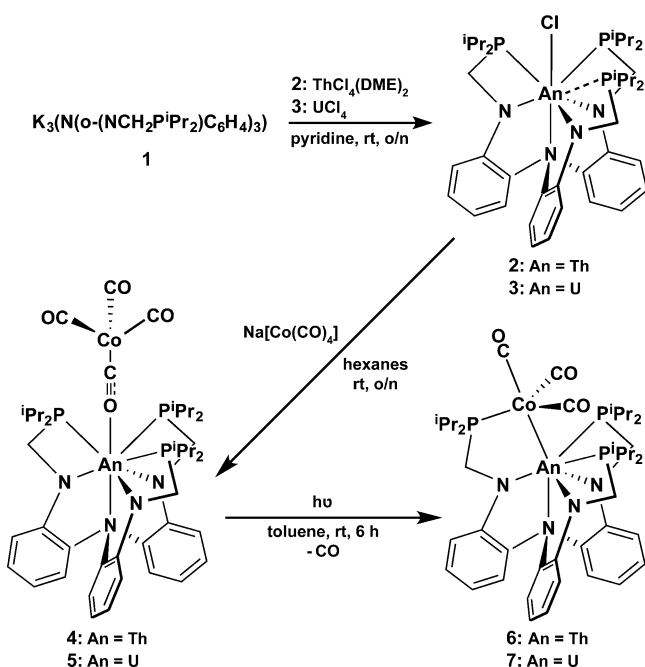
The first actinide–transition metal bond, between Th and Ru, was reported by Marks and co-workers nearly 30 years ago.¹⁴ In spite of this, *f*-element metal–metal bonds are still rare in comparison to the multitude of examples for the *s*, *p*, and *d* block.^{15–17} This is due in part to the fact that, while there are a broad range of synthetic routes to metal–metal bonds involving transition metals in particular,¹⁷ the synthesis of actinide analogues has been limited to salt metathesis and elimination reactions. Accordingly, a relatively small number of

examples has been reported,¹⁸ establishing uranium bound to iron, ruthenium, rhenium, and cobalt, in addition to the first example involving thorium.^{19–25} Expanding synthetic routes to actinide metal–metal bonds provides an exciting opportunity to develop this field, with the potential to offer new insight into electronic structure and yield alternative modes of bimetallic cooperativity for novel catalytic applications.

The modular nitrogen/phosphorus scaffold, N[*o*-(NHCH₂PⁱPr₂)C₆H₄]₃ (N₄P₃), has recently been shown to facilitate metal–metal bonding via stabilization through a secondary phosphine coordination sphere and has thus far been used to couple aluminum and chromium with a series of first row transition metals.^{26–28} Here, we show how this hard/soft donor system can be employed to provide a platform for bonding between (hard) actinides and (soft) late transition metals. Two important features of this approach are (i) the intermediacy of an isocarbonyl [Co(CO)₄][−] species that loses CO upon photolysis and (ii) the trapping of the resulting coordinatively unsaturated Co center by a pendent phosphine to yield the metal–metal-bonded products. A series of uranium complexes, as well as their diamagnetic thorium analogues, has been synthesized. To the best of our knowledge, this method represents a new route to actinide–transition metal bonds and

Received: December 28, 2013

Published: February 5, 2014

Scheme 1. Synthesis of Thorium and Uranium Complexes 2–7^a

^aDifferences in phosphine binding in complexes 2 and 3 are indicated by a dotted line.

results in a rare example of a U–Co bond as well as the first structurally characterized Th–Co bond. Additionally, these molecules allow for the electronic structure, solution state behavior, and magnetic properties of a new series of low-valent actinides to be studied.

RESULTS AND DISCUSSION

Synthesis and Structural Properties. The potassium salt of the pro-ligand, $\text{K}_3\{\text{N}[\text{o}-(\text{NCH}_2\text{P}^i\text{Pr}_2)\text{C}_6\text{H}_4]_3\}$ (**1**), was prepared by reaction of the triamine with $\text{K}[\text{N}(\text{TMS})_2]$ in toluene, affording the desired product in quantitative yield. Attempts to use the known lithium analogue were less successful, presumably due to salt incorporation—a common problem in metathesis chemistry with actinide metals.⁸ A uranium starting platform, as well as the diamagnetic thorium analogue, were targeted to allow for a wider range of characterization methods. Accordingly, the complexes $\{\text{N}[\text{o}-(\text{NCH}_2\text{P}^i\text{Pr}_2)\text{C}_6\text{H}_4]_3\}\text{ThCl}$ (**2**) and $\{\text{N}[\text{o}-(\text{NCH}_2\text{P}^i\text{Pr}_2)\text{C}_6\text{H}_4]_3\}\text{UCl}$ (**3**) were synthesized via combination of **1** with $\text{ThCl}_4(\text{DME})_2$ ²⁹ and UCl_4 ,³⁰ respectively, in pyridine (Scheme 1). Both reactions were stirred at room temperature overnight, resulting in a pale-yellow solution for the thorium complex **2**, and a dark-red solution for uranium complex **3**. Evaporation of the solvent under vacuum, followed by crystallization from a mixture of diethyl ether (Et_2O) and hexanes at -40°C , afforded colorless needles of **2** (65% yield) and orange needles of **3** (68% yield).

The molecular structure of complex **2**, as determined by X-ray diffraction, reveals the coordination about the metal center to be roughly trigonal dodecahedral (Figure 1a). As with the main group and transition metal N_4P_3 counterparts,^{26–28} phosphine coordination is metal-center dependent. The phosphine arms interact with the actinide centers to varying degrees, in addition to the four nitrogen donors of the ligand,

consistent with the much larger coordination sphere of the actinides. All three phosphines bind to the thorium center in **2**, but only two of the phosphine arms are coordinated in **3** (Figure 1b). This is consistent with the difference in ionic radii (1.00 \AA vs 1.05 \AA for $\text{U}(\text{IV})$ and $\text{Th}(\text{IV})$, respectively).³¹ Despite the small disparity, this variation is often enough to allow for a higher coordination number in the latter.¹ Complexes **2** and **3** represent a limited number of actinide complexes that employ ligands containing both hard and soft donors. Utilizing similar ligand frameworks, highly reactive intermediates have been stabilized for further functionalization with transition metals and lanthanides, meaning **2** and **3** could provide a unique opportunity to establish orthogonal reactivity patterns using actinides.^{32,33}

As an initial foray into exploring the capability of this platform to facilitate actinide metal–metal bonding, secondary metals known to bind favorably to the phosphine donors were targeted. Treatment of **2** or **3** with $\text{Na}[\text{Co}(\text{CO})_4]$ in hexanes at room temperature overnight (Scheme 1) resulted in precipitation of the desired products from solution; crystallization from a mixture of toluene and hexanes at -40°C yielded colorless blocks of **4** (77% yield) and dark-orange blocks of **5** (76% yield). While there is well-established literature precedent

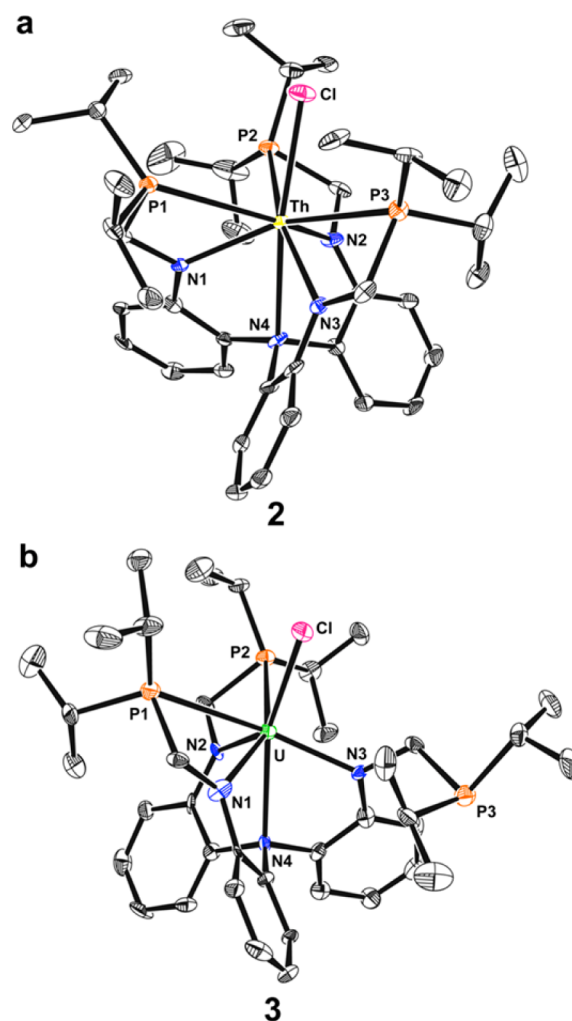


Figure 1. (a) Molecular structure of thorium complex **2**. (b) Molecular structure of uranium complex **3**. Thermal ellipsoids are set to a 50% probability level, and hydrogen atoms have been omitted for clarity.

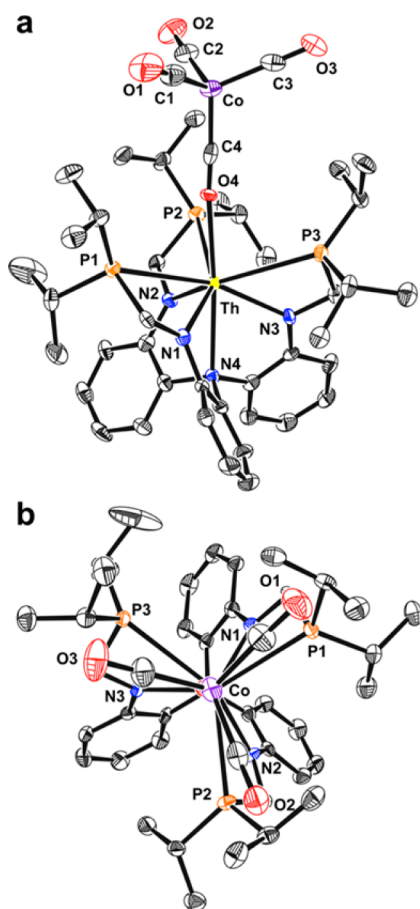


Figure 2. (a) Molecular structure of thorium complex 4. (b) Alternate view of 4 along the Co(μ -CO)Th axis, illustrating the partially staggered propeller conformation. Thermal ellipsoids are set to a 50% probability level, and hydrogen atoms have been omitted for clarity.

for carbonyl substitution by phosphines,^{34,35} the oxophilicity of the actinide centers, coupled with the inherent stability of the $[\text{Co}(\text{CO})_4]^-$ fragment, gave rise to less conventional isocarbonyl compounds 4 and 5, as revealed by X-ray diffraction studies (Figures 2 and S1). Although there are many heterobimetallic transition metal isocarbonyls,^{34,35} there are only five structurally characterized uranium isocarbonyls,^{24,36,37} and we are unaware of any reports for thorium. Uniquely, 4 and 5 provide heterobimetallic systems suited to photolytic substitution via the carbonyls, while also possessing a secondary coordination sphere capable of stabilizing resulting unsaturated intermediates.

The actinide centers for 4 and 5 are eight-coordinate, with all four nitrogens and the three phosphorus donors bound to the metal centers. Each complex displays a partially staggered conformation in relation to the $\text{Co}(\text{CO})_3$, N_3An , and P_3An units, respectively (Figure 2b). The helical twist along the $\text{An}-(\mu\text{CO})-\text{Co}$ axis results in torsion angles ranging from 23.43° to 33.44° , presumably to help minimize steric repulsions upon formation of the heterobimetallics.³⁸ The bond lengths and angles observed for 4 and 5 (Table S1 in Supporting Information [SI]) compare well with related uranium isocarbonyls, as well as a Yb compound having an analogous isocarbonyl bridged cobalt unit.³⁹

Actinide–transition metal bonds were targeted via UV irradiation of compounds 4 and 5 as shown in Scheme 1. Unlike the bulk of literature concerning photolysis of transition

metal carbonyl compounds, which describes either the irradiation of an existing metal–metal bond to promote dissociation or the facilitation of ligand exchange,^{34,35,40} irradiation of compounds 4 and 5 results in the formation of an actinide–metal bond (Figures 3 and S2 in SI). Evaporation of the solvent under vacuum, followed by crystallization from a mixture of Et_2O and hexanes at -40°C , afforded colorless needles of 6 (61% yield) and red needles of 7 (58% yield).

Formation of metal–metal bonds by this route is unusual for transition metals and, to our knowledge, has not been reported for actinides.^{41–43} Subjecting the isolated compounds 4 and 5 to subsequent irradiation under the same conditions does not result in further carbonyl ligand substitution. Additionally, 6 and 7 do not react with CO under either thermal or photochemical conditions to reform 4 and 5.

These compounds represent a unique system for comparing the variation in $\text{An}-\text{M}$ bonding involving two different actinides with identical coordination spheres. The geometry about the metal centers is approximately trigonal bipyramidal, with τ values of 0.88 and 0.85 for the thorium and uranium complexes, respectively.⁴⁴ The actinide–cobalt bond length is $3.0771(5)$ Å for 6 and $3.0319(7)$ Å for 7. The sums of the covalent radii for thorium and cobalt and uranium and cobalt are 2.86 Å and 2.81 Å, respectively.⁴⁵ While longer than expected, the U–Co distance is within the range of limited examples present in the literature ($2.9450(9)$ Å and $3.0812(7)–2.874(3)$);^{25,46} there are no data to compare with in the case of Th–Co. The difference in bond lengths between 6 and 7 is consistent with the disparity in radii (either ionic or covalent) between thorium and uranium.

Interestingly, one of the cis carbonyls in each complex is tilted slightly toward the actinide center. The interaction, which does not appear to be a crystal packing effect, is more pronounced in the thorium example as indicated by both the Co–C2 ($1.742(4)$ Å and $1.750(7)$ Å) and $\text{An}-\text{C}2$ ($3.094(4)$ Å and $3.198(1)$ Å) distances in 6 and 7, respectively, perhaps reflecting simply the difference in radii. Similar behavior has been observed for related carbonyl complexes with early transition metals.^{38,47}

NMR Spectroscopy. The thorium complex 2 shows a ^1H NMR spectrum indicative of three-fold symmetry in solution (assignments were confirmed by phosphorus decoupled and

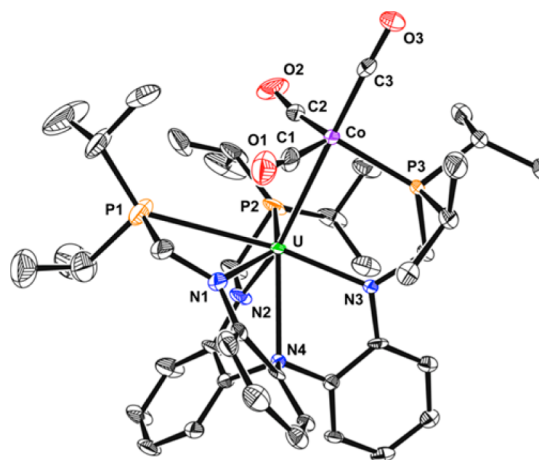


Figure 3. Molecular structure of uranium complex 7. Thermal ellipsoids are set to a 50% probability level, and hydrogen atoms have been omitted for clarity.

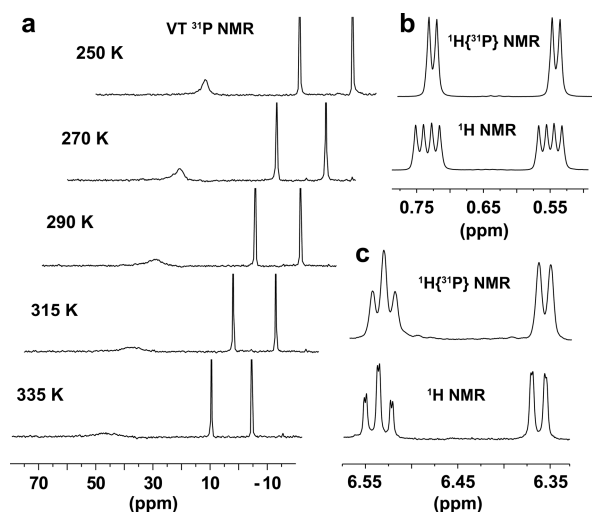


Figure 4. (a) Variable temperature ^{31}P NMR spectra of complex 6. (b) $^1\text{H}\{^{31}\text{P}\}$ (top) and ^1H NMR (bottom) spectra of two methyl groups of complex 4. (c) $^1\text{H}\{^{31}\text{P}\}$ (top) and ^1H NMR (bottom) spectra of two aromatic protons of complex 2. Both b and c illustrate the effect of phosphorus coupling observed in the ^1H NMR of the series.

proton–proton COSY NMR). However, unlike the analogous Al and Cr compounds of the N_4P_3 ligand,^{25–27} the methylene protons are diastereotopic, appearing as two doublets at 3.89 ($J = 12$ Hz) and 3.23 ($J = 12$ Hz) ppm. Additionally, all proton peaks show coupling to phosphorus, a feature that appears unique to the actinide compounds (Figure 4b and c). The ^{31}P NMR further confirms the three-fold symmetry, with a single resonance at 4.83 ppm. While the ^1H NMR spectrum for 3 is broad, paramagnetically shifted, and lacking any coherent splitting, the number of signals is in agreement with the symmetry observed in the thorium analogue. A phosphorus signal could not be detected, as is common in the presence of an f^2 uranium center (see below).²⁵

Much like the starting chloride complex 2, the solution-state behavior of the thorium isocarbonyl 4 is indicative of three-fold symmetry, with the ^1H NMR resonances resembling those seen for 2. The methylene protons remain diastereotopic at 3.55 ($J = 12$ Hz) and 3.05 ppm ($J = 12$ Hz), respectively, again likely a result of phosphine coordination to the thorium center. There is a single ^{31}P NMR peak that is shifted from 4.83 ppm for 2 to 6.41 ppm for 4, indicating a small deshielding effect, presumably due to a slightly stronger interaction of the actinide center with the carbonyl. Similar to complex 3, the ^1H NMR spectrum for 5 is broad, paramagnetically shifted, and lacks coherent splitting, but the number of signals is in agreement with the symmetry observed in the thorium analogue. Likewise, the ^{31}P spectrum is featureless due to paramagnetism.

The solution state behavior of the metal–metal bonded species 6 proves more complicated than either precursor, but upon careful inspection reflects the coordination seen in the solid state. The three-fold symmetry observed in thorium compounds 2 and 4 is absent for 6. Instead, NMR spectroscopy indicates a loss of symmetry resulting from the coordination of a phosphine arm to the cobalt center upon loss of CO. Where there had previously been only one resonance per proton group (i.e., aromatic, methylene, methine, and isopropyl) in compounds 2 and 4, three signals are observed in 6. Accordingly, there are three signals in the ^{31}P NMR at 44.59, 9.43, and -6.59 ppm. The downfield resonance is broad but in

Table 1. Selected FTIR Data for Complexes 4–7 and Related Compounds^a

cmpd	$\nu_{\text{CO}}(\text{cm}^{-1})$
free CO	2143
$\text{Na}[\text{Co}(\text{CO})_4]$	2024, 1878
4	2016, 1923, 1732
5	2013, 1922, 1748
6	1978, 1905, 1858
7	1977, 1907, 1864

^aCollected as Nujol mulls between KBr plates.

good agreement with phosphorus shifts reported for similar cobalt compounds.^{38,48} Variable-temperature experiments reveal a further broadening of the signal at higher temperatures and a sharpening at low temperatures (Figure 4a). Given the shift, and the dissimilarity from the other two signals, it seems likely that the broad signal corresponds to a cobalt-bound phosphine. The fluxional behavior could be due to an exchange of the ligand between the cobalt and the thorium, or the result of a Berry pseudorotation involving the carbonyls. Inequivalence of the remaining phosphorus atoms reflects the two different chemical environments observed in the solid-state structure. The features of the ^1H and ^{31}P NMR spectra for complex 7 are analogous to those described for paramagnetic complexes 3 and 5, with the exception that, like complex 6, the asymmetry of 7 results in a tripling of the peaks.

Infrared Spectroscopy. In addition to providing a facile platform for exploring photolytic chemistry, the carbonyls of complexes 4–7 also supply a useful spectroscopic handle to examine structural aspects of this series. Solid-state IR spectra of compounds 4 and 5 show two sharp CO stretches (Table 1) consistent with the approximate C_{3v} symmetry of the cobalt fragment seen in the crystal structures. Additionally, there is a broad stretch for the bridging carbonyls of 4 and 5 at 1732 and 1748 cm^{-1} , respectively. The dramatic weakening in the energy of this stretch is consistent with the electronic redistribution required to form the bridge and is similar to the few examples reported for actinides mentioned previously. The terminal CO stretches observed for 4 and 5 are significantly lower in energy than those seen in the cobalt starting material, indicating a significant redistribution of negative charge throughout the $[\text{Co}(\text{CO})_4]^-$ unit via cobalt–carbonyl backbonding. This is also reflected in the expanding and contracting respectively of the C–O and Co–C distances of the end-on carbonyl groups, as well as the C4–O4 and Co–O4 values of the isocarbonyl (Table S1 in SI).

Electronic redistribution is also evident in the solid-state IR spectra of compounds 6 and 7, which show three sharp CO stretches consistent with the geometry and CO coordination number to the cobalt unit seen in the crystal structure. The CO stretch of the carbonyl trans to the metal–metal bond (1858 and 1864 cm^{-1} for 6 and 7, respectively) provides a probe of the interaction strength and is indeed the only stretch with a significant disparity between the two complexes.³⁸ The strength of the carbonyl stretch should be affected by the bonding in the An–Co–CO linkage. The stronger the An–Co interaction, the weaker the Co–CO backbonding, and hence the stronger C–O stretching frequency. The C–O stretch of 7 has a higher frequency than 6, indicating the U–Co interaction is stronger than that of the Th–Co. Additionally, the stretches for 6 and 7 are weaker than for those of their isocarbonyl counterparts, consistent with a polarization of charge from the cobalt to the

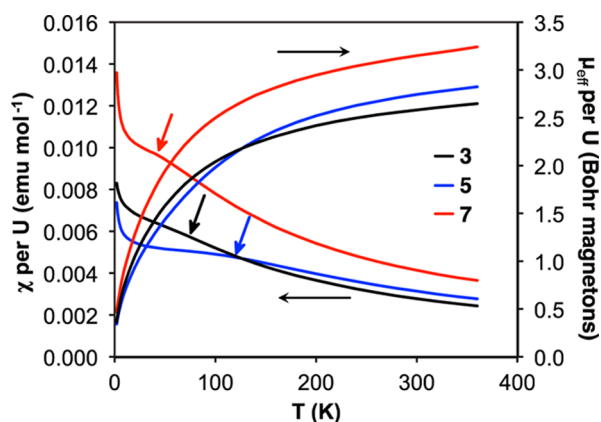


Figure 5. Variable-temperature magnetic susceptibility of complexes 3, 5, and 7. Note: vertical arrows indicate the change in slope due to thermal population of the first excited state.

actinide center and a corresponding decrease in Co–CO backbonding.

Magnetic Susceptibility. As an additional means of evaluating the electronic structure of the uranium series, variable-temperature magnetic susceptibilities (χ) of complexes 3, 5, and 7 were measured in the solid state (Figure 5). The effective magnetic moments of 3, 5, and 7 at 300 K are 2.6, 2.7, and 3.2 Bohr magnetons (μ_B), respectively. These values are lower than the free ion magnetic moment of both U(III) and U(IV), which is 3.6 μ_B in both cases.⁴⁹ Both crystal field splitting and covalency can affect the magnetic moment, making the room temperature moment alone insufficient in determining the uranium oxidation state. The observed values are similar to those reported for both U(III) and U(IV) amide complexes.^{49–54}

For 3, 5, and 7, μ_{eff} decreases toward zero as the temperature is lowered, which is consistent with U(IV), having an f^2 , 3H_4 configuration and a singlet ground state.¹ The temperature-independent ground state is indicated in the χ vs T plot by a change in slope (indicated with vertical arrows in Figure 5) where the first excited state becomes thermally populated. In 5, the ground state is least magnetic and is the only appreciably populated state up to ~ 100 K. In 3, the ground state has a greater magnetic susceptibility and persists to a somewhat lower temperature, ~ 70 K. In 7, the ground state has the greatest magnetic susceptibility and persists to ~ 60 K.

Both the magnetic susceptibility of the singlet state and the temperature over which this state is exclusively occupied are functions of the strength of the crystal field. Stronger ligands lead to larger splitting between the ground state and higher-lying states, decreasing the susceptibility of the ground state and increasing the temperature over which it is solely occupied. The splitting of the 3H_4 state is greatest in 5 and smallest in 7. This mirrors the bond distances observed between the uranium center and the apical ligand with the shortest (U–OC) in 5 and longest (U–Co) in 7. In agreement with the crystallographic and NMR data presented previously, this suggests that the isocarbonyl displays the strongest interaction with the U(IV) center and that Co has the weakest. This in turn underscores the necessity to employ photolytic excitation to enable the formation of the An–Co bond via ligand exchange.

UV–vis/NIR Spectroscopy. Finally, the electronic structure of the uranium series was investigated using UV–vis/NIR spectroscopy (Figure 6). Complexes 3, 5, and 7 display a broad

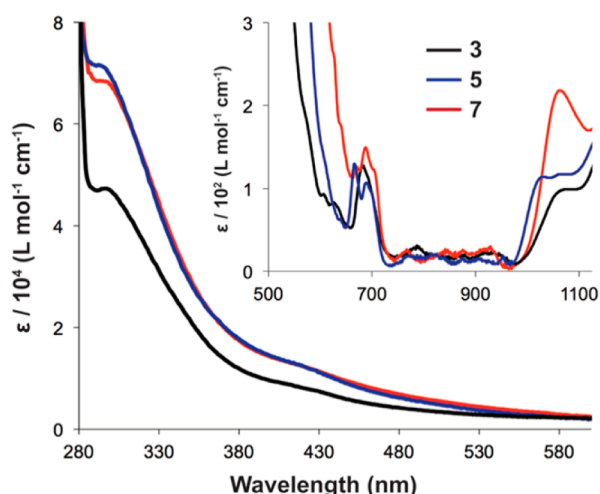


Figure 6. UV–visible absorption spectra of complexes 3, 5, and 7 in toluene. Inset: NIR absorption spectra of complexes 3, 5, and 7 in toluene.

shoulder at ~ 300 nm, followed by a peak at ~ 430 nm, showing shifts in agreement with the gradual orange-to-red color change observed across the series. Both peaks are similar to those reported for the analogous Al and Cr compounds of the ligand and are consistent with π – π^* transitions in the ligand backbone and M–L charge transfer, respectively.^{26–28} Additionally, there are several sharp peaks not seen in the main group or transition metal compounds at ~ 675 nm ($\epsilon = \sim 1.25 \times 10^2 \text{ M}^{-1} \text{ cm}^{-1}$), consistent with f -based transitions.

In contrast to the UV–vis region, the broad peaks in the NIR spectra are distinct between compounds. The uranium chloride complex 3 displays a single peak at 1064 nm ($\epsilon = 0.97 \times 10^2 \text{ M}^{-1} \text{ cm}^{-1}$) similar to that reported for the aluminum–cobalt complex. However, the isocarbonyl complex 5 displays two peaks at 1024 nm ($\epsilon = 1.12 \times 10^2 \text{ M}^{-1} \text{ cm}^{-1}$) and 1056 nm ($\epsilon = 1.17 \times 10^2 \text{ M}^{-1} \text{ cm}^{-1}$), and the U–Co bound complex 7 displays a more intense single peak at 1058 nm ($\epsilon = 2.16 \times 10^2 \text{ M}^{-1} \text{ cm}^{-1}$). Metal-based transitions were observed in the NIR region for the corresponding main group and transition metal examples of this ligand. Likewise, the two peaks observed for isocarbonyl 5 may arise due to independent cobalt- and uranium-based transitions. Subsequently, and consistent with a polarization of charge between the metal centers in 7, a single transition of increased intensity is seen upon formation of the U–Co bond.

CONCLUSIONS

These studies have demonstrated that actinide–transition metal bonds can be formed via photolysis of heterobimetallic isocarbonyl complexes. A key design feature of this work is the ready availability of a pendent phosphine ligand that is unique to the N_4P_3 ligand scaffold. The secondary coordination sphere incorporated into this ligand framework is crucial to the formation of actinide–metal bonds upon photolysis since without it the resulting coordinatively unsaturated $\text{Co}(\text{CO})_3$ complex would likely decompose. In this way, we have generated two new An–Co complexes, including one featuring a previously unknown Th–Co bond. Additionally, this series of complexes provides important experimental data relating to coordination environments, oxidation states, and bonding of what is still a relatively limited number of actinide–transition metal compounds. We believe this approach represents a new

way to create actinide–metal bonds and may yield a rich platform for expanding the study of actinide metal–metal bonding and associated reactivity.

EXPERIMENTAL DETAILS

General Procedures. Unless otherwise noted, all reactions were performed using standard Schlenk line techniques, or in an MBraun N₂-atmosphere glovebox (<1 ppm O₂/H₂O). All glassware and Celite were stored in an oven at ~150 °C. Dimethoxyethane (DME), diethyl ether (Et₂O), toluene, hexanes, pentane, and pyridine were dried and degassed using a Phoenix Solvent Drying System commercially available from JC Meyer Solvent Systems. Hexamethyldisiloxane (HMDSO) was vacuum-transferred from CaH₂ and degassed by bubbling N₂ through the solution. Deuterated solvents were vacuum-transferred from either sodium/benzophenone (C₆D₆ and toluene-*d*₈) or CaH₂ (pyridine-*d*₅) and degassed with three freeze–pump–thaw cycles. All NMR spectra were recorded at the specified temperature on Bruker AVQ-400, DRX 500, or AV-600 spectrometers. Temperature calibration was performed using changes in chemical shift separation of ethylene glycol at high temperature, and methanol at low temperature. ¹H chemical shifts (δ) were calibrated using residual solvent peaks. ³¹P chemical shifts (δ) were referenced to an external standard (Ph₃PO at 23 ppm). UV–visible and near-infrared (NIR) spectra were collected in toluene and determined with a UV-3101PC scanning spectrophotometer, using a Schlenk-adapted 1 mm quartz cell. Infrared (IR) spectra were recorded with a Thermo Scientific Nicolet iS10 FTIR spectrophotometer as Nujol mulls between KBr plates. Melting points were determined on an Optmelt SRS using sealed capillaries prepared under nitrogen and are uncorrected. Photolysis was conducted using a Rayonet reactor (model RPR-100) centered at 253 nm with approximately 1.65 × 10¹⁶ photons/s/cm². The ligand N[*o*-(NCH₂PⁱPr₂)C₆H₄]₃,²⁵ ThCl₄(DME)₂,²⁹ UCl₄,³⁰ and Na[Co(CO)₄]⁵⁵ were prepared according to literature procedures.

K₃[N[*o*-(NCH₂PⁱPr₂)C₆H₄]₃] (1). A solution of the ligand N[*o*-(NCH₂PⁱPr₂)C₆H₄]₃ (2.0 g, 2.9 mmol) in toluene (40 mL) was added to a suspension of K[N(TMS)₂] (1.9 g, 9.7 mmol) in toluene (40 mL) to produce a yellow solution. The reaction mixture was stirred for 1 d, resulting in the precipitation of a yellow solid. The reaction mixture was filtered and washed with hexanes (2 × 5 mL) to afford the desired product as a pale-yellow solid (2.33 g, 99% yield). ¹H NMR (400 MHz, pyridine-*d*₅, 293 K): δ 7.24 (d, 1H, Ar-*H*, *J* = 8.0 Hz), 7.04 (t, 1H, Ar-*H*, *J* = 8.0 Hz), 6.47 (d, 1H, Ar-*H*, *J* = 8.0 Hz), 5.93 (t, 1H, Ar-*H*, *J* = 8.0 Hz), 3.42 (ABq, 2H, CH₂, Δδ_{AB} = 0.13, *J*_{AB} = 16 Hz), 1.77 (m, 2H, CH), 1.11 (m, 12H, CH₃). ³¹P NMR (400 MHz, pyridine-*d*₅): δ 2.00. Mp: dec >164 °C.

{N[*o*-(NCH₂PⁱPr₂)C₆H₄]₃}ThCl (2). A solution of 1 (1.1 g, 1.4 mmol) in pyridine (25 mL) was added to a suspension of ThCl₄(DME)₂ (766 mg, 1.4 mmol) in pyridine (25 mL) to produce an off-white suspension. The reaction mixture was stirred for 12 h, resulting in a pale-yellow solution. The solvent was removed in vacuo to yield a pale-orange solid. The solid was extracted with Et₂O (3 × 10 mL), filtered, and concentrated until saturation. Hexanes were added dropwise until cloudy, and the solution was then chilled for 2 d at –40 °C to afford the product as colorless needles (843 mg, 65% yield). Single crystals suitable for X-ray diffraction were obtained from a concentrated solution of 2 in pentane stored at –40 °C for 12 h. ¹H NMR (600 MHz, C₆D₆, 293 K): δ 7.18 (t, partially obscured by solvent, 1H, Ar-*H*, *J* = 6.0 Hz), 7.07 (d, 1H, Ar-*H*, *J* = 12 Hz), 6.53 (t, 1H, Ar-*H*, *J* = 9.0 Hz), 6.36 (d, 1H, Ar-*H*, *J* = 6.0 Hz), 3.89 (d, 1H, CH₂, *J* = 12 Hz), 3.23 (d, 1H, CH₂, *J* = 12 Hz), 2.06 (sept, 1H, CH, *J* = 6.0 Hz), 1.57 (sept, 1H, CH, *J* = 6.0 Hz), 1.27 (d, 3H, CH₃, *J* = 6.0 Hz), 1.24 (d, 3H, CH₃, *J* = 6.0 Hz), 0.84 (d, 3H, CH₃, *J* = 6.0 Hz), 0.66 (d, 3H, CH₃, *J* = 6.0 Hz). ³¹P NMR (600 MHz, C₆D₆, 293 K): δ 4.83. Anal. Calcd (%) for C₃₉H₆₀ClN₄P₃Th: C, 49.55; H, 6.40; N, 5.93. Found: C, 49.17; H, 6.69; N, 5.82. Mp: dec >138 °C.

{N[*o*-(NCH₂PⁱPr₂)C₆H₄]₃}UCl (3). A solution of 1 (1.0 g, 1.3 mmol) in pyridine (25 mL) was added to a suspension of UCl₄ (480 mg, 1.3 mmol) in pyridine (25 mL) to produce a red suspension. The reaction mixture was stirred for 12 h, resulting in a dark-red solution. The

solvent was removed in vacuo to yield a dark-orange solid. The solid was extracted with Et₂O (3 × 10 mL), filtered, and concentrated until saturation. Hexanes were added dropwise until cloudy, and the solution was then chilled for 1 d at –40 °C to afford the product as orange needles (807 mg, 68% yield). Single crystals suitable for X-ray diffraction were obtained from a concentrated solution of 3 in pentane stored at –40 °C for 12 h. ¹H NMR (400 MHz, C₆D₆, 293 K): δ 37.92 (s, br), 22.49 (s, br), 11.58 (s, br), 10.91 (s, br), 9.41 (s, br), 8.67 (m, br), 7.03 (s, br), 5.65 (s, br), 1.22 (m, br), –2.70 (s, br), –4.82 (s, br), –6.64 (s, br). UV–vis/NIR [nm, ε (M^{–1} cm^{–1})]: 298, 47,100; 431, 7,320; 680, 129; 1064, 97. Anal. Calcd (%) for C₃₉H₆₀ClN₄P₃U: C, 49.23; H, 6.36; N, 5.89. Found: C, 49.34; H, 6.45; N, 6.01. Mp: dec >145 °C. μ_{eff} = 2.6 μ_B at 300 K.

{N[*o*-(NCH₂PⁱPr₂)C₆H₄]₃}Th(μ-OC)Co(CO)₃ (4). A solution of 2 (100 mg, 0.10 mmol) in toluene (2 mL) was added to a suspension of Na[Co(CO)₄] (21 mg, 0.10 mmol) in toluene (2 mL) to produce a pale-yellow suspension. The reaction mixture was stirred for 12 h, resulting in a yellow solution and a fine white precipitate. The solvent was removed in vacuo to yield an off-white solid. The solid was extracted with toluene (3 × 2 mL), filtered, and concentrated until saturation. Hexanes were added dropwise until cloudy, and the solution was then chilled for 1 d at –40 °C to afford the product as colorless blocks (88 mg, 77% yield). Single crystals suitable for X-ray diffraction were obtained from a concentrated solution of 4 in toluene stored at –40 °C for 12 h. ¹H NMR (600 MHz, C₆D₆, 293 K): δ 7.08 (t, 1H, Ar-*H*, *J* = 9.0 Hz), 7.02 (d, 1H, Ar-*H*, *J* = 6.0 Hz), 6.51 (t, 1H, Ar-*H*, *J* = 9.0 Hz), 6.11 (d, 1H, Ar-*H*, *J* = 6.0 Hz), 3.55 (d, 1H, CH₂, *J* = 12 Hz), 3.05 (d, 1H, CH₂, *J* = 12 Hz), 2.15 (sept, 1H, CH, *J* = 6.0 Hz), 1.46 (sept, 1H, CH, *J* = 6.0 Hz), 1.31 (d, 3H, CH₃, *J* = 6.0 Hz), 1.28 (d, 3H, CH₃, *J* = 6.0 Hz), 0.77 (d, 3H, CH₃, *J* = 6.0 Hz), 0.59 (d, 3H, CH₃, *J* = 6.0 Hz). ³¹P NMR (600 MHz, C₆D₆, 293 K): δ 6.41. IR (cm^{–1}): 2016 (m, CO), 1923 (s, CO), 1733 (s, CO), 1586 (m), 1310 (m), 1290 (m), 1234 (w), 1157 (w), 1116 (w), 1040 (w), 745 (m), 722 (m), 563 (m), 512 (m). Anal. Calcd (%) for C₄₃H₆₀CoN₄O₄P₃Th: C, 47.78; H, 5.60; N, 5.18. Found: C, 35.29; H, 3.63; N, 5.09. The isocarbonyl compounds are subject to very rapid thermal and photolytic decomposition unless kept frozen and in a dark environment. Therefore it is unsurprising that the found percentages for elemental analysis are not in good agreement. Mp: dec >136 °C.

{N[*o*-(NCH₂PⁱPr₂)C₆H₄]₃}U(μ-OC)Co(CO)₃ (5). A solution of 3 (330 mg, 0.34 mmol) in toluene (2 mL) was added to a suspension of Na[Co(CO)₄] (66 mg, 0.34 mmol) in toluene (2 mL) to produce an orange suspension. The reaction mixture was stirred for 12 h, resulting in a red solution and a fine white precipitate. The solvent was removed in vacuo to yield an orange solid. The solid was extracted with toluene (3 × 2 mL), filtered, and concentrated until saturation. Hexanes were added dropwise until cloudy, and the solution was then chilled for 1 d at –40 °C to afford the product as orange blocks (281 mg, 76% yield). Single crystals suitable for X-ray diffraction were obtained from a concentrated solution of 5 in toluene stored at –40 °C for 12 h. ¹H NMR (400 MHz, C₆D₆, 293 K): δ 52.86 (s, br), 23.92 (s, br), 16.58 (s, br), 12.66 (m, br), 10.29 (s, br), 8.39 (m, br), 8.31 (s, br), 3.44 (m, br), 0.29 (s, br), –2.04 (m, br), –3.13 (s, br), –12.93 (s, br). IR (cm^{–1}): 2013 (m, CO), 1922 (s, CO), 1748 (s, CO), 1586 (m), 1310 (m), 1290 (m), 1234 (w), 1157 (w), 1116 (w), 1049 (w), 747 (m), 722 (m), 560 (m), 517 (m). UV–vis/NIR [nm, ε (M^{–1} cm^{–1})]: 296, 71,100; 429, 13,100; 668, 127; 693, 104; 1024, 112; 1056, 117. Anal. Calcd (%) for C₄₃H₆₀CoN₄O₄P₃U: C, 47.52; H, 5.56; N, 5.16. Found: C, 41.34; H, 3.86; N, 4.83. Mp: dec >149 °C. μ_{eff} = 2.7 μ_B at 300 K.

{N[*o*-(NCH₂PⁱPr₂)C₆H₄]₃}ThCo(CO)₃ (6). A solution of 4 (130 mg, 0.12 mmol) in toluene (2 mL) was irradiated with ultraviolet light (centered at 254 nm) for 12 h, resulting in a color change from pale yellow to yellow. The solvent was removed in vacuo to yield a pale-yellow solid. The solid was extracted with Et₂O (3 × 2 mL), filtered, and concentrated until saturation. The solution was then chilled for 1 d at –40 °C to afford the product as colorless blocks (79 mg, 61% yield). Single crystals suitable for X-ray diffraction were obtained by vapor diffusion at –40 °C of hexane into a concentrated solution of 6 in toluene. ¹H NMR (600 MHz, C₆D₆, 293 K): δ 7.23 (t, 1H, Ar-*H*, *J* = 6.0 Hz), 7.19 (t, 1H, Ar-*H*, *J* = 6.0 Hz), 7.12 (m, 2H, Ar-*H*), 7.06 (d,

1H, Ar-H, $J = 6.0$ Hz), 6.95 (d, 1H, Ar-H, $J = 6.0$ Hz), 6.61 (m, 2H, Ar-H), 6.52 (t, 1H, Ar-H, $J = 6.0$ Hz), 6.49 (t, 1H, Ar-H, $J = 6.0$ Hz), 6.42 (d, 1H, Ar-H, $J = 6.0$ Hz), 6.14 (d, 1H, Ar-H, $J = 6.0$ Hz), 4.38 (d, 1H, CH₂, $J = 12$ Hz), 3.97 (d, 1H, CH₂, $J = 12$ Hz), 3.62 (d, 1H, CH₂, $J = 12$ Hz), 3.36 (m, 2H, CH₂), 3.14 (d, 1H, CH₂, $J = 12$ Hz), 2.43 (sept, 1H, CH, $J = 6.0$ Hz), 2.00 (sept, 1H, CH, $J = 6.0$ Hz), 1.87 (m, 2H, CH), 1.77 (sept, 1H, CH, $J = 6.0$ Hz), 1.57 (sept, 1H, CH, $J = 6.0$ Hz), 1.43 (d, 3H, CH₃, $J = 12$ Hz), 1.39 (d, 3H, CH₃, $J = 6.0$ Hz), 1.27 (d, 3H, CH₃, $J = 6.0$ Hz), 1.11 (d, 3H, CH₃, $J = 6.0$ Hz), 0.94 (m, 9H, CH₃), 0.86 (d, 3H, CH₃, $J = 6.0$ Hz), 0.81 (d, 3H, CH₃, $J = 12$ Hz), 0.74 (d, 3H, CH₃, $J = 6.0$ Hz), 0.62 (m, 6H, CH₃). ³¹P NMR (600 MHz, C₆D₆, 293 K): δ 44.59, 9.43, -6.59. IR (cm⁻¹): 1979 (s, CO), 1905 (s, CO), 1858 (s, CO), 1591 (m), 1310 (m), 1290 (m), 1254 (w), 1156 (w), 1117 (w), 1040 (w), 856 (w), 743 (m), 727 (m). Anal. Calcd (%) for C₄₂H₆₀CoN₄O₃P₃Th: C, 47.91; H, 5.74; N, 5.32. Found: C, 48.04; H, 5.86; N, 5.19. Mp: dec >160 °C.

{[N(o-NCH₂PPPr₂)C₆H₄]₃UCo(CO)₃} (7). A solution of 5 (150 mg, 0.14 mmol) in toluene (2 mL) was irradiated with ultraviolet light (centered at 254 nm) for 12 h, resulting in a color change from orange to red. The solvent was removed in vacuo to yield a red solid. The solid was extracted with Et₂O (3 × 2 mL), filtered, and concentrated until saturation. The solution was then chilled for 1 d at -40 °C to afford the product as red blocks (87 mg, 58% yield). Single crystals suitable for X-ray diffraction were obtained from a concentrated solution of 7 in HMDSO stored at -40 °C for 12 h. ¹H NMR (400 MHz, C₆D₆, 293 K): δ 88.56 (s, br), 75.00 (s, br), 51.45 (s, br), 38.96 (s, br), 28.70 (s, br), 27.11 (s, br), 20.06 (s, br), 17.34 (s, br), 17.05 (s, br), 16.45 (s, br), 16.05 (s, br), 14.41 (s, br), 11.84 (s, br), 11.72 (s, br), 11.29 (m, br), 11.10 (m, br), 9.17 (s, br), 8.32 (s, br), 7.91 (s, br), 7.52 (s, br), 6.42 (s, br), 3.39 (m, br), 2.68 (m, br), 2.17 (s, br), -1.84 (s, br), -2.05 (m, br), -9.41 (m, br), -10.95 (s, br), -11.57 (s, br), -11.79 (s, br), -15.67 (s, br), -19.01 (s, br), -24.40 (s, br), -26.25 (s, br). IR (cm⁻¹): 1977 (s, CO), 1908 (s, CO), 1864 (s, CO), 1590 (m), 1310 (m), 1288 (m), 1253 (w), 1155 (w), 1117 (w), 1048 (w), 846 (w), 742 (m), 722 (m). UV-vis/NIR [nm, ϵ (M⁻¹ cm⁻¹): 299, 69,800; 433, 10,900; 669, 124; 689, 149; 1058, 216. Anal. Calcd (%) for C₄₂H₆₀CoN₄O₃P₃U: C, 47.64; H, 5.71; N, 5.29. Found: C, 47.52; H, 5.79; N, 5.16. Mp: dec >145 °C. $\mu_{\text{eff}} = 3.0 \mu_{\text{B}}$ at 300 K.

Crystallographic Procedures. X-ray structural determinations were performed at CHEXRAY, University of California, Berkeley, on a Bruker APEX II Quazar diffractometer. The instrument is Kappa Geometry with DX, and is a three-circle diffractometer that couples a CCD detector⁵⁶ with a sealed-tube source of monochromatized Mo K α radiation. A crystal of appropriate size was coated in Paratone-N oil and mounted on a Kaptan loop. The loop was transferred to the diffractometer, centered in the beam, and cooled by a nitrogen flow low-temperature apparatus that had been previously calibrated by a thermocouple placed at the same position as the crystal. Preliminary orientation matrices and cell constants were determined by collection of 60 10 s frames, followed by spot integration and least-squares refinement. The reported cell dimensions were calculated from all reflections with $I > 10\sigma$. The data were corrected for Lorentz and polarization effects; no correction for crystal decay was applied. An empirical absorption correction based on comparison of redundant and equivalent reflections was applied using SADABS.⁵⁷ All software used for diffraction data processing and crystal-structure solution and refinement are contained in the APEX2 program suite (Bruker AXS, Madison, WI).⁵⁸ Thermal parameters for all non-hydrogen atoms were refined anisotropically. For all structures, $R1 = \sum(|F_o| - |F_c|) / \sum(|F_o|)$; $wR2 = [\sum\{w(F_o^2 - F_c^2)^2\} / \sum\{w(F_o^2)^2\}]^{1/2}$, ORTEP diagrams were created using the ORTEP-3 software package and POV-ray.^{59,60}

Magnetism Procedures. Uranium complexes 3, 5, and 7 (6.4 mg) were sandwiched between two plugs of quartz wool (Hereaus, 6.6 mg) in a 4 mm OD quartz tube, which was flame-sealed on both ends. Sample magnetization was recorded at 0.1 T, 0.5 T, and 1 T using a Quantum Designs MPMS SQUID magnetometer. Magnetization was corrected for the diamagnetism of the quartz wool using Pascal's constants (no correction for the diamagnetism of the quartz tube is needed as the quartz tube never leaves the SQUID coils). Molar susceptibility was corrected for the presence of a small amount of

ferromagnetic impurity (M_{ferro}), the diamagnetism of the quartz wool (χ_{QW}), ligands and uranium (χ_{dia}) using Pascal's constants, and calculated using the following equation:

$$\chi_{\text{mol}} = \frac{(\text{molecular weight})}{(\text{sample mass})} \left[\frac{M_{\text{meas}} - M_{\text{ferro}}}{H} - \chi_{\text{QW}} \right] - \chi_{\text{dia}}$$

where χ_{mol} is the molar susceptibility, M_{meas} is the measured magnetization, M_{ferro} is the magnetization of the ferromagnetic impurity, which is temperature independent and assumed to be identical at all fields, χ_{QW} is the contribution to the susceptibility due to the quartz wool, χ_{dia} is the diamagnetic correction, and H is the applied field. For 3 and 5, this equation was applied to the 0.5 and 1 T data to determine M_{ferro} which was 1.6×10^{-5} emu and 2.92×10^{-5} emu, respectively. The 0.1 T data was fit to the other data using $M_{\text{ferro},0.1\text{T}} = 0.63 M_{\text{ferro}}$ because the 0.1 T data is below the anisotropy field of the ferromagnetic impurity (see below); the value of 0.63 was determined by fitting the 0.1 T data to the 0.5 and 1 T data. For 7, the amount of ferromagnetic impurity was determined using the 0.1, 0.5, and 1 T data and $M_{\text{ferro},0.1\text{T}} = 0.63 M_{\text{ferro}}$; $M_{\text{ferro}} = 1.6 \times 10^{-5}$ emu.

Two ferromagnetic impurities are commonly encountered in laboratory samples, steel or iron metal and magnetite or other ferrites from oxide coating on stainless steel lab equipment. Of these, magnetite is far more likely to be encountered. In general, the magnetization of ferromagnets is temperature independent below the Curie temperature, which is 860 K for magnetite, so magnetization of the impurity is temperature independent for this experiment. The magnetization of ferromagnets is also largely field-independent above the anisotropy field, which is approximately 0.2 T for magnetite, above which the magnetization is ~ 90 emu/g.⁶¹ Below the anisotropy field, the magnetization of a magnet is roughly linear with applied field. On the basis of the assumption that the impurity is magnetite or some other ferrite resulting from the abrasion of stainless steel lab equipment, the data were corrected for a temperature- and field-independent ferromagnetic impurity. M_{ferro} was allowed to vary to minimize least-squares difference between χ_{mol} at different fields, which produced a saturation magnetization of $M_{\text{ferro}} \approx 2 \times 10^{-5}$ emu (actual values in SI), which corresponds to $\sim 0.2 \mu\text{g}$ of magnetite. Data before and after correction for the presence of the ferromagnetic impurity are shown in Figures S3–S8 in the SI.

■ ASSOCIATED CONTENT

● Supporting Information

The molecular structures of complexes 5 and 6, as well as crystallographic data and refinement parameters for complexes 2–7 (CIF), and additional magnetic susceptibility data. This material is available free of charge via the Internet at <http://pubs.acs.org>.

■ AUTHOR INFORMATION

Corresponding Author

arnold@berkeley.edu

Notes

The authors declare no competing financial interest.

■ ACKNOWLEDGMENTS

A.L.W. acknowledges the NSF for a GFRP fellowship and UC Berkeley for a Dissertation Year Fellowship. We are grateful to Antonio DiPasquale (XRD), Thomas Gianetti (NMR), and Nick Kornienko (NIR) for assistance with instrumentation, as well as Drs. Casey Brown and Stefan Minasian for helpful discussions. This work was supported by the U.S. Department of Energy, Office of Basic Energy Sciences, Chemical Sciences, Biosciences, and Geosciences Division, and a portion was performed at Lawrence Berkeley National Laboratory under Contract No. DE-AC02-05CH11231.

■ REFERENCES

- (1) Morss, L. R.; Edelstein, N.; Fuger, J. *The Chemistry of the Actinide and Transactinide Elements*, 3rd ed.; Springer: Dordrecht, The Netherlands, 2006.
- (2) Jones, M. B.; Gaunt, A. J. *Chem. Rev.* **2013**, *113*, 1137.
- (3) Liddle, S. T.; Mills, D. P. *Dalton Trans.* **2009**, *29*, 5592.
- (4) Ephritikhine, M. *Dalton Trans.* **2006**, *21*, 2501.
- (5) Minasian, S. G.; Krinsky, J. L.; Arnold, J. *Chem.—Eur. J.* **2011**, *17*, 12234.
- (6) Edelmann, F. T. *Coord. Chem. Rev.* **2013**, *257*, 1122.
- (7) Oelkers, B.; Butovskii, M. V.; Kempe, R. *Chem.—Eur. J.* **2012**, *18*, 13566.
- (8) Edelmann, F. T. *Synthetic Methods of Organometallic and Inorganic Chemistry*; Herrmann, W. A., Ed.; Thieme: New York, NY, 1997; Vol. 6.
- (9) *Spent Fuel Reprocessing Options*; International Atomic Energy Agency: Vienna, Austria, 2009.
- (10) *Nuclear Energy Advisory Committee Report*; U.S. Department of Energy: Washington, DC, 2008.
- (11) Kozimor, S. A.; Yang, P.; Batista, E. R.; Boland, K. S.; Burns, C. J.; Clark, D. L.; Conrad, S. D.; Martin, R. L.; Wilkerson, M. P.; Wolfsberg, L. E. *J. Am. Chem. Soc.* **2009**, *131*, 12125.
- (12) Arnold, P. L.; Turner, Z. R.; Kaltsayannis, N.; Pelekanaki, P.; Bellabarba, R. M.; Tooze, R. P. *Chem.—Eur. J.* **2010**, *16*, 9623.
- (13) Fox, A. R.; Bart, S. C.; Meyer, K.; Cummins, C. C. *Nature* **2008**, *455*, 341.
- (14) Sternal, R. S.; Brock, C. P.; Marks, T. J. *J. Am. Chem. Soc.* **1985**, *107*, 8270.
- (15) Green, S. P.; Jones, C.; Stasch, A. *Science* **2007**, *318*, 1754.
- (16) Schnöckel, H. *Dalton Trans.* **2008**, *33*, 4344.
- (17) Cotton, F. A.; Murillo, C. A.; Walton, R. A. *Multiple Bonds Between Metal Atoms*, 3rd ed.; Springer Science: New York, NY, 2005.
- (18) Based on a search of the *Cambridge Structural Database* for unsupported actinide–transition metal bonds. The latest update to the database at the time of writing was November 2013.
- (19) Bucaille, A.; Le Borgne, T.; Ephritikhine, M.; Daran, J. C. *Organometallics* **2000**, *19*, 4912.
- (20) Monreal, M. J.; Khan, S. I.; Kiplinger, J. L.; Diaconescu, P. L. *Chem. Commun.* **2011**, *47*, 9119.
- (21) Gardner, B. M.; McMaster, J.; Lewis, W.; Liddle, S. T. *Chem. Commun.* **2009**, *20*, 2851.
- (22) Patel, D.; King, D. M.; Gardner, B. M.; McMaster, J.; Lewis, W.; Blake, A. J.; Liddle, S. T. *Chem. Commun.* **2010**, *47*, 295.
- (23) Gardner, B. M.; Patel, D.; Cornish, A. D.; McMaster, J.; Lewis, W.; Blake, A. J.; Liddle, S. T. *Chem.—Eur. J.* **2011**, *17*, 11266.
- (24) Patel, D.; Moro, F.; McMaster, J.; Lewis, W.; Blake, A. J.; Liddle, S. T. *Angew. Chem., Int. Ed.* **2011**, *50*, 10388.
- (25) Napoline, J. W.; Kraft, S. J.; Matson, E. M.; Fanwick, P. E.; Bart, S. C.; Thomas, C. M. *Inorg. Chem.* **2013**, *52*, 12170.
- (26) Rudd, P. A.; Liu, S.; Gagliardi, L.; Young, V. G.; Lu, C. C. *J. Am. Chem. Soc.* **2011**, *133*, 20724.
- (27) Rudd, P. A.; Liu, S.; Planas, N.; Bill, E.; Gagliardi, L.; Lu, C. C. *Angew. Chem., Int. Ed.* **2013**, *52*, 4449.
- (28) Clouston, L. J.; Siedschlag, R. B.; Rudd, P. A.; Planas, N.; Hu, S.; Miller, A. D.; Gagliardi, L.; Lu, C. C. *J. Am. Chem. Soc.* **2013**, *135*, 13142.
- (29) Cantat, T.; Scott, B. L.; Kiplinger, J. L. *Chem. Commun.* **2010**, *46*, 919.
- (30) Kiplinger, J. L.; Morris, D. E.; Scott, B. L.; Burns, C. J. *Organometallics* **2002**, *21*, 5978.
- (31) Shannon, R. D. *Acta Crystallogr., Sect. A* **1976**, *32*, 751.
- (32) Scott, J.; Basuli, F.; Fout, A. R.; Huffman, J. C.; Mindiola, D. J. *Angew. Chem., Int. Ed.* **2008**, *47*, 8502.
- (33) Cantat, T.; Graves, C. R.; Scott, B. L.; Kiplinger, J. L. *Angew. Chem., Int. Ed.* **2009**, *48*, 3681.
- (34) Stiegman, A. E.; Tyler, D. R. *Coord. Chem. Rev.* **1985**, *63*, 217.
- (35) Meyer, T. J.; Caspar, J. V. *Chem. Rev.* **1985**, *85*, 187.
- (36) Gardner, B. M.; Lewis, W.; Blake, A. J.; Liddle, S. T. *Inorg. Chem.* **2011**, *50*, 9631.
- (37) Arnold, P. L.; Mansell, S. M.; Maron, L.; McKay, D. *Nat. Chem.* **2012**, *4*, 668.
- (38) Jansen, G.; Schubart, M.; Findeis, B.; Gade, L. H.; Scowen, I. J.; McPartlin, M. *J. Am. Chem. Soc.* **1998**, *120*, 7239.
- (39) Tilley, T. D.; Andersen, R. A. *Chem. Soc., Chem. Commun.* **1981**, *19*, 985.
- (40) Bentsen, J. G.; Wrighton, M. S. *J. Am. Chem. Soc.* **1987**, *109*, 4530.
- (41) Job, R. C.; Curtis, M. D. *Inorg. Chem.* **1973**, *12*, 2514.
- (42) Triplett, K.; Curtis, M. D. *Inorg. Chem.* **1976**, *15*, 431.
- (43) Knox, S. A. R.; Stone, F. G. A. *J. Chem. Soc., A* **1971**, *18*, 2874.
- (44) Addison, A. W.; Rao, T. N.; Reedijk, J.; van Rijn, J.; Verschoor, G. C. *J. Chem. Soc., Dalton Trans.* **1984**, *7*, 1349.
- (45) Pyykkö, P.; Atsumi, M. *Chem.—Eur. J.* **2009**, *15*, 186.
- (46) Mills, D. P.; Moro, F.; McMaster, J.; van Slageren, J.; Lewis, W.; Blake, A. J.; Liddle, S. T. *Nature Chem.* **2011**, *3*, 454.
- (47) Werle, C.; Bailly, C.; Karmazin-Brelot, L.; Le Goff, X.-F.; Ricard, L.; Djukic, J.-P. *J. Am. Chem. Soc.* **2013**, *135*, 17839.
- (48) Bungu, P. N.; Otto, S. *Dalton Trans.* **2011**, *40*, 9238.
- (49) King, D. M.; Lewis, W.; Liddle, S. T. *Inorg. Chim. Acta* **2012**, *380*, 167.
- (50) Lewis, A. J.; Williams, U. J.; Kikkawa, J. M.; Carroll, P. J.; Schelter, E. J. *Inorg. Chem.* **2012**, *51*, 37.
- (51) Weiss, C. J.; Marks, T. J. *Dalton Trans.* **2010**, *39*, 6576.
- (52) Castro-Rodriguez, I.; Olsen, K.; Gantzel, P.; Meyer, K. *J. Am. Chem. Soc.* **2003**, *125*, 4565.
- (53) Reynolds, J. G.; Zalkin, A.; Templeton, D. H.; Edelstein, N. M. *Inorg. Chem.* **1977**, *16*, 599.
- (54) Andersen, R. A. *Inorg. Chem.* **1979**, *18*, 1507.
- (55) Edgell, W. F.; Lyford, J., IV. *Inorg. Chem.* **1970**, *9*, 1932.
- (56) SMART: *Area Detector Software Package*; Bruker Analytic X-ray Systems I.: Madison WI, 2003.
- (57) SADABS: *Bruker-Nonius Area Detector Scaling and Absorption V2.05*; Bruker Analytical X-ray System I.: Madison WI, 2003.
- (58) Sheldrick, G. M. *Acta Crystallogr., Sect. A* **2008**, *64*, 112.
- (59) Farrugia, L. J. *Appl. Crystallogr.* **1997**, *30*, S65.
- (60) van der Sluis, P.; Spek, A. L. *Acta Crystallogr.* **1990**, *A46*, 194.
- (61) Morales, M. A.; Jain, T. K.; Labhasetwar, V.; Leslie-Pelecky, D. L. *J. Appl. Phys.* **2005**, *97*, 10Q905.